

FIBRE-OPTIC SENSORS

https://doi.org/10.1070/QEL16523

Detection of electric current pulses by a fibre-optic sensor using spun fibre

Ya.V. Przhiyalkovsky, V.P. Gubin, N.I. Starostin, S.K. Morshnev, A.I. Sazonov

Abstract. **We have studied distinctive features of the response of a fibre-optic current sensor with a spun-fibre sensing loop to short current pulses. It has been shown theoretically that, in a reflective interferometer, the polarisation mode dispersion (PMD) in the sensing spun fibre has no effect on the pulsed output signal of the sensor, in contrast to the PMD in a connecting fibre line. The response of the current sensor to a rectangular pulse has linear edges and its duration is determined by the relationship between the current pulse duration and the light propagation time in the spun fibre. The transition from a linear edge to the maximum sensor response is not accompanied by any transient process. The maximum response amplitude corresponds to the response to an equivalent direct current at a current pulse duration exceeding the light propagation time in the spun fibre. The present calculation results and experimental data agree well for current pulses longer than 300 ns at a light propagation time in the spun fibre of ~1 μs.**

Keywords: *spun optical fibre, fibre-optic sensor, response, current pulse, Faraday effect.*

1. Introduction

At present, Faraday effect fibre-optic current sensors (FOCS's) have attractive engineering, performance and environmental characteristics and are being used increasingly in electric power engineering and electrometallurgy for accurate dc and low-frequency current measurements [1, 2]. Other potential application areas of FOCS's are related to the short response time of the magneto-optical Faraday effect ($\sim 10^{-9}$ s), which allows such sensors to be used for accurate pulsed current measurements, e. g. in pulsed linear electron accelerators and plasma heating and compression systems [3–5]. In designing such FOCS's, it is necessary to take into account the physical factors that influence the shape of current pulses. However, these issues have not yet been addressed in sufficient detail. In particular, for assessing the accuracy of FOCS's it is important to know the duration of the transient process for the sensor response to a change in current. In particular, Pimenov and Kazachkov [5] assume that, to ensure accurate current pulse amplitude measurements, the current pulse duration should far exceed the propagation time of light in the sensing loop, but this constraint needs to be substantiated. A number of studies [6–8] were concerned with the limitations on the upper limit of the frequency band of FOCS's due to the finite time of light propagation through the fibre of the sensing element (transit mechanism).

At present, the most promising FOCS configuration is a reflective interferometer with a sensing loop based on fibre with a helical structure of built-in linear birefringence (spun optical fibre) [9, 10]. Spun fibre possesses a number of unique polarisation properties related to the rotation of their birefringence (BR) axes. On the one hand, their BR imparts to them a certain polarisation stability to external mechanical influences [11, 12]. On the other, if the BR beat length L_b considerably exceeds the spin pitch L_s of the BR axes, the helical structure of the fibre makes it possible to maintain light ellipticity in it near a circular polarisation state, which is necessary for the effective Faraday phase shift accumulation [10–12].

Another polarisation property of spun fibre is polarisation mode dispersion (PMD), which leads to different propagation velocities of orthogonally polarised optical waves, with a Faraday phase shift accumulating between them (PMD mechanism). Because of this, one distinctive feature of pulsed current measurements using FOCS's, related to the use of spun fibre as a sensing element, is a possible effect of PMD on the response shape and magnitude. This issue has not yet been addressed in the literature. The purpose of this work is to study the physical mechanisms determining the shape of the output signal of reflective interferometer-based FOCS's using spun fibre in the detection of short current pulses.

2. Theory

The distinctive features of polarisation evolution for light propagating in media with a helical birefringence structure (in particular, in spun fibre) in a steady state have been studied in sufficient detail [13–19]. The main conclusions necessary for theoretical substantiation of pulsed FOCS operation are presented briefly in Appendix.

Light propagating in spun fibre of length L is a linear combination of orthogonal elliptically polarised modes, u and v, whose azimuths rotate together with the BR axes (screw modes) [17]. For $L_s/2L_b \ll 1$, the ellipticity of these modes is near unity (quasi-circular modes). In this approximation, the refractive indices of the modes, $n_{u,v}$, are given by

$$n_{u,v} \approx \bar{n} \pm \frac{\sigma\beta}{4k_0} \pm \frac{\gamma}{2k_0} = \bar{n}_{u,v} \pm \frac{\gamma}{2k_0}, \qquad (1)$$

Ya.V. Przhiyalkovsky, V.P. Gubin, N.I. Starostin, S.K. Morshnev, A.I. Sazonov V.A. Kotel'nikov Institute of Radio Engineering and Electronics (Fryazino Branch), Russian Academy of Sciences, pl. Vvedenskogo 1, 141190 Fryazino, Moscow region, Russia; e-mail: yankus.p@gmail.com, nis229@ire216.msk.su

Received 25 September 2017
Kvantovaya Elektronika **48** (1) 62–69 (2018)
Translated by O.M. Tsarev

where $\bar{n}$ is the effective refractive index of the fundamental mode in the fibre with no allowance for anisotropy; $\bar{n}_{u,v} = n_{u,v}(\gamma = 0)$ are the refractive indices of the modes in the absence of a magnetic field; $\beta = k_{sl} - k_f = k_0(n_{sl} - n_f)$ is the difference between the propagation constants of the slow and fast linearly polarised waves in a thin layer of the fibre, which is determined by the built-in linear BR $n_{sl} - n_f$; $k_0 = \omega/c$; $\omega = 2\pi c/\lambda$ is the frequency of the light; λ is its wavelength; c is the speed of light in vacuum; $\gamma = k_r - k_l = 2VB_z$ is the Faraday effect-induced difference between the propagation constants of the circularly polarised modes; V is the Verdet constant of the fibre material; B_z is the magnetic induction vector component along the light propagation direction; and $\sigma = L_s/(2L_b)$. Note that the difference between the refractive indices of modes u and v is of the order of λ/L_b.

In the geometric optics approximation, the spatiotemporal (t, z) trajectories of light rays propagating in spun fibre are determined by the equation of propagation [20]

$$\frac{dz}{dt} = \frac{c}{n}, \tag{2}$$

into which $n_{u,v}$ from (1) should be substituted. In the absence of a magnetic field, integrating (2), we obtain

$$\bar{z}_{u,v}(t) = \frac{c(t - t_{0u,v})}{\bar{n}_{u,v}}, \tag{3}$$

where we introduce times zero, at which the light rays emerge from the origin: $t_{0u,v}$. This is necessary for taking into account the PMD in the connecting line through which light is coupled into the spun fibre. The waves pass the entire path L in a time $\tau_{u,v} = \bar{n}_{u,v}L/c$.

Note first of all that, in the general case of the transient magnetic field of a current pulse, γ and, in turn, $n_{u,v}$ are functions of both time t and coordinate z (the path passed by the ray). Because of this, the variables in Eqn (2) can only be separated in some particular cases. At the same time, since the Faraday effect is weak, the z-coordinate in the function $\gamma(t, z)$ can be replaced, with a sufficient degree of accuracy, by the coordinate $\bar{z}_{u,v}(t)$, corresponding to the propagation of rays in the absence of a magnetic field. As a result, the refractive indices $n_{u,v}$ become functions of time: $n_{u,v} = n_{u,v}(t, \bar{z}_{u,v}(t))$.

Consider the phase shift between waves u and v propagating in spun fibre over length L in the circular polarisation approximation. Waves u and v arrive at the point $z = L$ with time delays $\Delta t_{u,v}$ relative to the propagation time of a light ray in the absence of a magnetic field. Then, integrating the equations of propagation (2) for waves u and v we obtain

$$L = \int_0^L dz = \int_{t_0}^{t_{0u,v}+\tau_{u,v}+\Delta t_{u,v}} \frac{c\,dt}{n_{u,v}} \approx \frac{c\tau_{u,v}}{\bar{n}_{u,v}} + \frac{c\Delta t_{u,v}}{\bar{n}_{u,v}} \mp \frac{c}{2k_0\bar{n}_{u,v}^2} \times \int_{t_{0u,v}}^{t_{0u,v}+\tau_{u,v}} \gamma(t, \bar{z}_{u,v})\,dt, \tag{4}$$

where we take into account that $\gamma \ll k_0\bar{n}_{u,v}$ because of the small magnitude of the Faraday effect. Using (4), we find $\Delta t_{u,v}$:

$$\Delta t_{u,v} = \pm\frac{1}{2k_0\bar{n}_{u,v}} \int_{t_{0u,v}}^{t_{0u,v}+\tau_{u,v}} \gamma(t, \bar{z}_{u,v})\,dt. \tag{5}$$

As a result, the total time delay between the waves at the point $z = L$ is given by

$$\Delta t = t_{0u} + \tau_u + \Delta t_u - (t_{0v} + \tau_v + \Delta t_v) = \Delta t_0 + \frac{(\bar{n}_u - \bar{n}_v)L}{c} + \frac{1}{2k_0\bar{n}_u}\int_{t_{0u}}^{t_{0u}+\tau_u} \gamma(t, \bar{z}_u)\,dt + \frac{1}{2k_0\bar{n}_v}\int_{t_{0v}}^{t_{0v}+\tau_v} \gamma(t, \bar{z}_v)\,dt. \tag{6}$$

Given that $\bar{n}_u - \bar{n}_v = \sigma\beta/(2k_0)$, the phase shift can be determined as

$$\Delta\varphi = \omega\Delta t = \omega\Delta t_0 + \frac{\sigma\beta L}{2} + \frac{c}{2\bar{n}_u}\int_{t_{0u}}^{t_{0u}+\tau_u} \gamma(t, \bar{z}_u)\,dt + \frac{c}{2\bar{n}_v}\int_{t_{0v}}^{t_{0v}+\tau_v} \gamma(t, \bar{z}_v)\,dt. \tag{7}$$

In (7), the first and second constant terms are determined by the PMD of the connecting fibre line (which leads to different ray entrance times, $t_{0u} \neq t_{0v}$) and the PMD of the spun fibre ($\bar{n}_u \neq \bar{n}_v$), respectively. The last two terms are the integrals of the functions $\gamma = (t, \bar{z}_{u,v}(t))$ along the time window of ray propagation and determine the Faraday phase shifts for each wave. Replacing time integration by integration with respect to the coordinate, we can rewrite the same expression in the form

$$\Delta\varphi = \omega\Delta t_0 + \frac{\sigma\beta L}{2} + \frac{1}{2}\int_0^L \gamma\left(\frac{z\bar{n}_u}{c} + t_{0u}, z\right)dz + \frac{1}{2}\int_0^L \gamma\left(\frac{z\bar{n}_v}{c} + t_{0v}, z\right)dz. \tag{8}$$

Note that the main contribution to the final phase shift (at $\Delta t_0 = 0$) is made by the second term in (7) and (8). For example, in the case of a spun fibre with a built-in BR beat length $L_b = 9$ mm and spin pitch $L_s = 3$ mm, this term is about 19π m^{-1}, whereas even in considerable magnetic fields (at electric currents of hundreds of amperes) the phase shift 2π between circularly polarised light waves in silica fibre arises at fibre lengths of tens of metres or more.

Below, expressions (7) and (8), derived for light propagating through spun fibre in the forward direction, are considered in greater detail for some particular cases:

1. The absence of PMD in the sensing fibre under consideration ($\bar{n}_u = \bar{n}_v = \bar{n}$), which corresponds in the limit ($\beta \to 0$) to isotropic fibre. If there is also no PMD in the connecting fibre line before the fibre under consideration, so that $t_{0u} = t_{0v}$, there is no constant term in the phase shift. At the same time, the integrals in (7) and (8), which determine the Faraday phase shift of each wave, are calculated along the same path in the tz plane, so they are identical.

2. If the fibre under consideration has no PMD ($\bar{n}_u = \bar{n}_v = \bar{n}$), but there is PMD in the connecting fibre line [for example, if it is based on a linear polarisation-maintaining (PM) fibre], the former arguments of the integrands in (8) are shifted in time. Because of this, the waves (u and v) generally have different Faraday phase shifts. For example, in the case of a reflective configuration in which light is reflected from a mirror at the end of the fibre under consideration and then travels backwards, the time delay of polarisation mode propagation in the connecting line (PMD) may lead to a 'temporal splitting' of the output signal of the current sensor interferometer (see below for details).

3. In the most general case, when there is PMD in both the connecting line and the fibre under consideration (spun fibre), both constant terms in (7) and (8) differ from zero. The Faraday phase shifts of the waves are then calculated by integration along different paths in the tz plane. As a result, the waves make different contributions to the resultant phase shift.

4. In the case of spun fibre, the integrals in (7) and (8) coincide only at a constant current. This is well demonstrated by formula (8), where the former argument of the function γ is independent of z.

For further analysis of the output signal of a reflective interferometer, consider light propagation after reflection from the mirror at the end of the spun fibre. The phase shift between the backward-propagating waves can be found by replacing σ with $-\sigma$ in all the expressions derived above. As a result, the constant phase shift defined by the second term in (7) and (8) is compensated. Since the light propagating backwards in the connecting line has an orthogonal polarisation mode, the constant phase shift due to the PMD in the connecting line is also compensated after the light passes the entire optical path in the forward and backward directions. As a result, the total phase shift between the operating waves in the case of a spatially uniform external magnetic field of a current (i.e. when γ is independent of the latter argument: $\gamma(t,z) = \gamma(t) = 2VB_z(t)$) can be found, to first order in $\sim\lambda/L_b$, as

$$\Delta\varphi \approx \frac{Vc}{\bar{n}}\left(\int_{t_{0u}}^{t_{0u}+2\tau} B_z(t)\,\mathrm{d}t + \int_{t_{0v}}^{t_{0v}+2\tau} B_z(t)\,\mathrm{d}t\right), \qquad (9)$$

where $\tau = \bar{n}L/c$ is the light propagation time in one direction in an isotropic fibre with a refractive index $\bar{n}$. If there is no PMD in the connecting line, $t_{0uv} = t_0$, the expression for the total phase shift simplifies to

$$\Delta\varphi \approx \frac{2Vc}{\bar{n}}\int_{t_0}^{t_0+2\tau} B_z(t)\,\mathrm{d}t. \qquad (10)$$

In particular, in the case of a direct current and closed fibre loop, we obtain $\Delta\varphi = 4VB_zL = 4VI_0$ [9, 12]. Note that this expression completely coincides with an analogous expression derived for an isotropic fibre with a refractive index $\bar{n}$. Thus, due to the reflective interferometer configuration, the PMD of the spun fibre has a negligible effect (to first order in $\sim\lambda/L_b$) in the case under consideration.

3. Current pulse detection by a low-coherence reflective interferometer

Consider how a low-coherence reflective interferometer detects a single rectangular current pulse of amplitude I_0 and duration T, beginning at time $t' = 0$ (here and in what follows, primes refer to the time measured from the beginning of the current pulse). Figure 1 shows a simplified schematic of the interferometer. The components important for subsequent analysis are the connecting line (*4*) and the sensing fibre loop (*6*) with a mirror (*7*). The connecting line can be made from both PM and spun fibre. If the connecting line is based on PM fibre, a wave plate is mounted at the input of the sensing loop. A current-carrying conductor (*8*) is placed in the centre of the loop. Two orthogonal linearly polarised light waves having equal intensities are launched into the fibre line (*4*) through the common interferometer input/output (*1*) and a polariser (*2*). A quarter-wave plate (*5*) converts the linear polarisations of the waves into circular ones. In the loop (*6*), the circularly polarised light waves acquire Faraday phase shifts proportional to the magnetic field of the current. After reflection from the mirror (*7*), the waves pass the optical path in the backward direction and the result of their interference is recorded by a photodetector (not shown in Fig. 1).

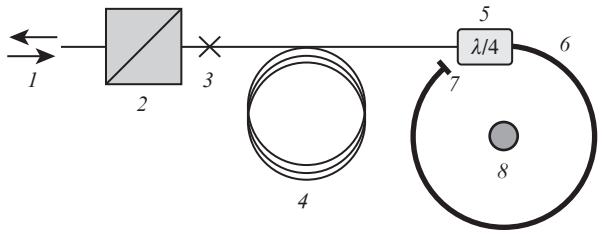

Figure 1. Simplified schematic of the current sensor interferometer: (*1*) light input/output; (*2*) polariser; (*3*) oriented fusion splice (45° between the BR axes); (*4*) PM fibre of the connecting line; (*5*) quarter-wave plate; (*6*) sensing loop; (*7*) mirror; (*8*) current-carrying conductor.

Consider now the case when the longitudinal component B_z of the external magnetic field generated by a current is constant throughout the spun fibre at a given instant in time. In practice, this can be ensured e.g. by coiling the spun fibre around a current-carrying conductor perpendicular to the plane of the loop. The time dependence $\gamma(t) \sim B_z(t)$ is then rectangular in shape.

The propagation of light waves in spun fibre can be illustrated by $t-z$ diagrams, which show the trajectories of rays entering the spun fibre at different instants of time. The trajectories are solutions to the equation $\mathrm{d}t/\mathrm{d}z = n/c$, the inverse of Eqn (2), and the slope α of such a trajectory is determined by the refractive index n. The trajectory of wave u in $t-z$ diagrams will be shown by a solid line, and that of wave v, by a dashed line. The backward propagation of the waves will be treated as a continuation of their forward propagation from the mirror to the interferometer output with the corresponding replacement of the refractive indices: $n_{u,v} \leftrightarrow n'_{v,u}$ (and $n_{\mathrm{sl,f}} \leftrightarrow n_{\mathrm{f,sl}}$ for the PM fibre in the connecting line). Note also that, in all the figures below, the slopes of trajectories are shown substantially different for clarity of illustration, whereas actually the angle difference is small: $\Delta\alpha \approx (n_u - n_v)/c \approx \beta\sigma/(2k_0) \ll \bar{n}/c$.

3.1. Configuration with no connecting line (no delay)

Figure 2 shows ray propagation diagrams in the tz plane for a configuration with no connecting line. The shaded area in Fig. 2 corresponds to the region where light waves propagating in the spun fibre interact with the magnetic field generated by a current pulse of duration T (which begins at $t' = 0$). The time dependences of the phase shifts (9), corresponding to the $t-z$ ray propagation diagrams, in terms of time t' can be calculated by the formula

$$\Delta\varphi(t') = \frac{2Vc}{\bar{n}}\int_{-2\tau}^{0} B_z(t-t')\,\mathrm{d}t = \frac{2VcB_0}{\bar{n}}\int_{-2\tau}^{0}\Pi(t-t',\,T)\,\mathrm{d}t \qquad (11)$$

and are presented in the left panels in Fig. 2. Here, B_0 is the longitudinal magnetic induction component corresponding to

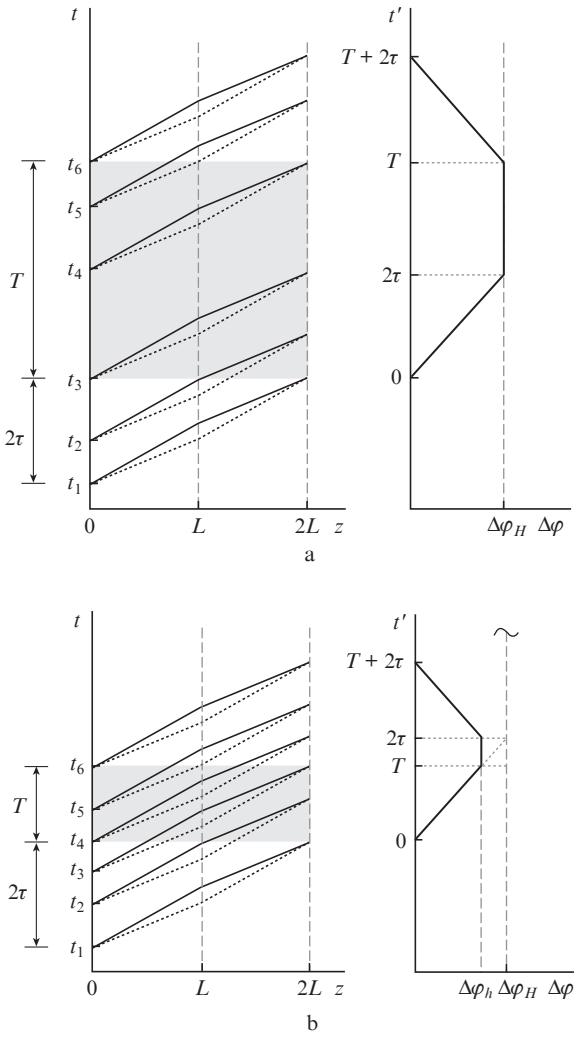

Figure 2. Spatiotemporal diagrams illustrating phase shift accumulation during the detection of a rectangular current pulse of duration (a) $T > 2\tau$ and (b) $T < 2\tau$.

a given current I_0 and the function $\Pi(t, T)$ is unity for $0 \leqslant t \leqslant T$ and zero elsewhere.

It is seen from the diagrams in Fig. 2 that the magnetic field of the current influences the phase difference between the rays that emerged from the source in the time range $t_1 \leqslant t \leqslant t_6$. In the case of a long current pulse ($T > 2\tau$, Fig. 2a), the rays that emerged at time t_1 will arrive at the end of the spun fibre exactly at time $t_3 = t_1 + 2\tau$, when the current will be turned on. Starting at this instant of time, there will be a signal at the photodetector output, as shown in the right panel in Fig. 2a. All the rays that emerged from the source in the time range $t_1 \leqslant t \leqslant t_3 = t_1 + 2\tau$ will accumulate the phase shift only in that part of their trajectory lying in the shaded area. Since the trajectory in the tz plane is linear with high accuracy, the accumulated phase shift will also increase linearly for time 2τ. The waves that emerged in the time range $t_3 \leqslant t \leqslant t_4 = t_3 + (T - 2\tau)$ accumulate the Faraday phase shift throughout their propagation, so the output signal will be constant for time $T - 2\tau$, $\Delta\varphi_H = 4VNI_0$, where N is the number of turns in the fibre coil, i.e. the signal will be equal to the response to an equivalent direct current. In the time interval $t_4 \leqslant t \leqslant t_6 = t_4 + 2\tau$, the situation will be opposite to that in the initial step: the rays will only partially accumulate the phase shift, which will be smaller for the rays that emerged later. Finally, the rays that emerged in the range $t > t_6$ will not interact with the magnetic field of the current pulse and the output signal will be zero starting at time $t_6 + 2\tau$. It is worth noting that transitions from the edges to the top are sharp (with no gradual transition).

It is seen in Fig. 2b that, for $T < 2\tau$, because of the short pulse duration none of the rays accumulates the Faraday phase shift throughout its propagation. In particular, the rays that emerge in the time range $t_3 \leqslant t \leqslant t_4 = t_3 + (2\tau - T)$ accumulate the phase shift during only a part $(T/2\tau)$ of their propagation time. Accordingly, the ratio of the maximum output signal to the signal corresponding to the shift $\Delta\varphi_H$ at the direct current I_0 will also be $T/2\tau$. The output signal increases and decreases at the same rate, but for time $T < 2\tau$.

3.2. Configuration with a connecting line (with a delay)

Figure 3 shows $t-z$ diagrams illustrating phase shift accumulation for each wave and the shape of the resultant output signal at a particular length, $l > 0$, of a PM fibre-based connecting line. In this case, because of the different light propagation velocities in the PM fibre of the connecting line (PMD in the fibre), the waves will arrive at the beginning of the spun fibre at different instants of time. As a result, the time intervals $T + 2\tau$ during which the waves interact with the magnetic field of the current pulse and generate an output signal will be displaced relative to each other (see the output signal in the right of Fig. 3). Moreover, the contribution of each wave to the output signal will lag the beginning of the current pulse, $t' = 0$, because after interactions in the spun fibre the light passes the delay line in the backward direction. The delay times t'_{sl} and t'_{f} are determined by the light propagation times along the slow and fast BR axes of the PM fibre in the backward direction: $t'_{\mathrm{sl,f}} = n_{\mathrm{sl,f}}l/c$. Figure 4 shows the contributions of the two waves to the shape of the resultant output signal at different delay line lengths. Thus, the overall delay of the response of the system is t'_{f} and the time shift between the output signals of the two waves is $\Delta t' = t'_{\mathrm{sl}} - t'_{\mathrm{f}} = l(n_{\mathrm{sl}} - n_{\mathrm{f}})/c$. In particular, at a sufficiently long delay line length, when $\Delta t' \geqslant T + 2\tau$, the output signal splits into two components and its amplitude decreases twofold.

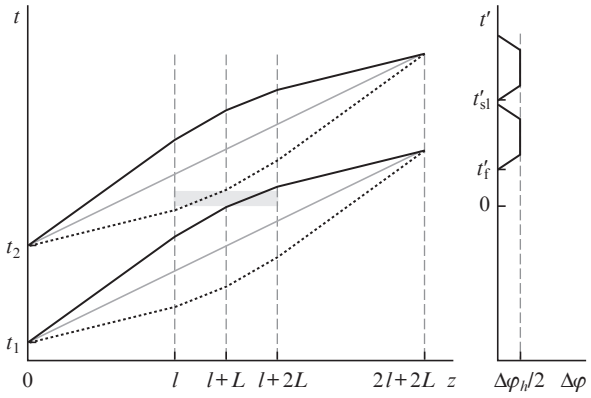

Figure 3. Spatiotemporal diagram illustrating phase shift accumulation during the detection of a rectangular current pulse in a configuration with a connecting line.

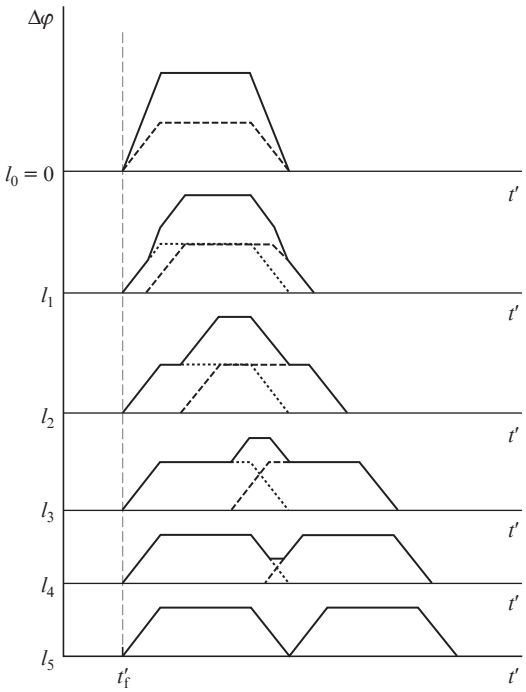

Figure 4. Time diagram of the phase shift during the detection of a rectangular current pulse in a configuration with a connecting line (with a delay) for lengths $l_0 < l_i < l_5$ ($i = 1–4$) and $l_5 = c(T + 2\tau)/(n_{s1} - n_f)$.

4. Experimental setup

Figure 5 shows a schematic of the experimental setup, which is a simplified version of a reflective interferometer-based FOCS and includes a rectangular current pulse generator and oscilloscope. The FOCS comprises a superluminescent light source (*1*) with a centre wavelength of 1550 nm and bandwidth of 20 nm, directional coupler (*2*), polariser (*3*), discrete Faraday rotator (*4*), connecting fibre line (*5*), sensing fibre coil (*6*) and Fresnel reflector (*7*) on its end. The sensing coil was placed in a toroidal copper wire solenoid (*9*), through which a rectangular electric current pulse (*8*) produced by a generator (*12*) was passed. The time constant of the current-controlling circuit ($\tau_{LR} \approx 50$ ns) was determined by a resistor (*10*). The current pulse shape was controlled using a small resistance (*11*). Using the rotator (*4*), the operating point of the interferometer was displaced by 90°. The output signal of the interferometer was detected by a photodetector (*14*). The time constant of the photodetector, τ_{ph}, was ~75 ns. The sensing coil and connecting line were made using spun fibre with a built-in linear BR beat length $L_b = 9$ mm and spin pitch $L_s = 3$ mm. To reduce the effect of magnetic interference from the current being measured on the connecting line, it had the form of a multiturn coil. In this study, we used a short (~10 m) line. The spun fibre of the sensing coil was wound onto a 20-mm-long, 14-mm-diameter bobbin with a number of turns $N_1 = 2000$. The number of turns of the solenoid was $N_2 = 25$. The calculated double pass time 2τ of light in the coil was 1120 ns.

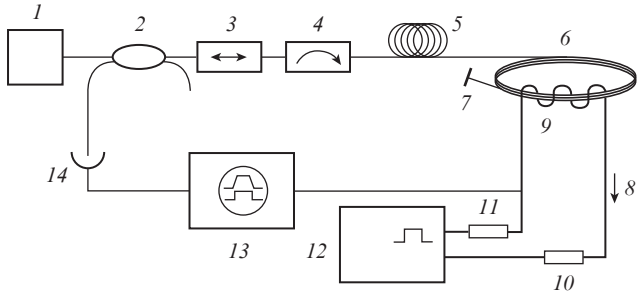

Figure 5. Schematic of the experimental setup:
(*1*) light source; (*2*) coupler; (*3*) polariser; (*4*) Faraday rotator; (*5*) connecting fibre line; (*6*) measuring fibre coil; (*7*) mirror; (*8*) current being measured; (*9*) solenoid; (*10*) current-controlling resistor; (*11*) control resistor; (*12*) rectangular current pulse generator; (*13*) dual-beam oscilloscope; (*14*) photodetector.

The output signal of the sensor, proportional to the phase shift $\Delta\varphi$ and, accordingly, to the current pulse amplitude, was picked up at the photodetector output. The characteristic of the interferometer was not linearised because signals corresponded to small Faraday phase shifts (under 0.1 rad). Its sensitivity was calibrated by comparing the amplitudes of pulsed signals and the output signal from an equivalent direct current.

5. Results and discussion

Figure 6 shows the shapes of a current pulse (lower trace) and the output signal of the sensor (upper trace) at a single current pulse duration in the solenoid $T = 2000$ ($T > 2\tau$), 1120 ($T = 2\tau$) and 500 ns ($T < 2\tau$) and a current through the solenoid $I_0 = 133$ mA. In our experiments, the inverse of the duty factor was 1000. Figure 7 shows the measured relative amplitude $\Delta\varphi_h/\Delta\varphi_H$ and relative full width at half maximum $T_{1/2}/(2\tau)$ of the detected pulses as functions of the relative current pulse duration $T/(2\tau)$. The dashed lines represent calculation results. Measurement accuracy was determined by the signal to noise ratio.

Consider first a factor related to the finite time of interaction between the light and the magnetic field of the current. The FOCS response $\Delta\varphi$ to a single rectangular current pulse has the shape of an isosceles trapezium, which degenerates into a triangle at $T = 2\tau$ (see Fig. 6b). The response edges have the form of a linear function with a slope proportional to the current pulse amplitude. At $T \geqslant 2\tau$, the edge width τ_{ed} is equal to the light propagation time in the spun fibre: $\tau_{ed} = 2\tau$. At $T < 2\tau$, we have $\tau_{ed} = T$. The response amplitude at $T \geqslant 2\tau$ is equal to the response to an equivalent direct current: $\Delta\varphi = \Delta\varphi_H = 4VN_1N_2I_0$. At $T < 2\tau$, it decreases as $\Delta\varphi_h = \Delta\varphi_H(T/2\tau)$ at a given pulse amplitude, which leads to an increased uncertainty in current pulse amplitude measurements. The present experimental data are in satisfactory agreement with calculation results. Since in our calculations the transition from a linear edge to a flat top has no transient process, the experimentally observed transient process of reaching a maximum response of duration $\tau_{adj} \approx 250$ ns has an instrumental origin. It is determined by the time constant of the photodetector, $\tau_{ph} \approx 75$ ns, and the width of the current pulse edges, which are in turn determined by the time constant of the LR circuit ($\tau_{LR} \approx 50$ ns).

The instrumental time constants have a significant effect on the shape of the FOCS response if they are comparable to the current pulse duration. The effect shows up first of all as a distortion of the flat top of the response trapezium (see Fig. 6c). It is important to note that the transient process has no effect on the maximum FOCS response if the current pulse being detected has a rectangular shape at $T > \tau_{adj}$. This is confirmed by measurements of the full width at half maximum of the

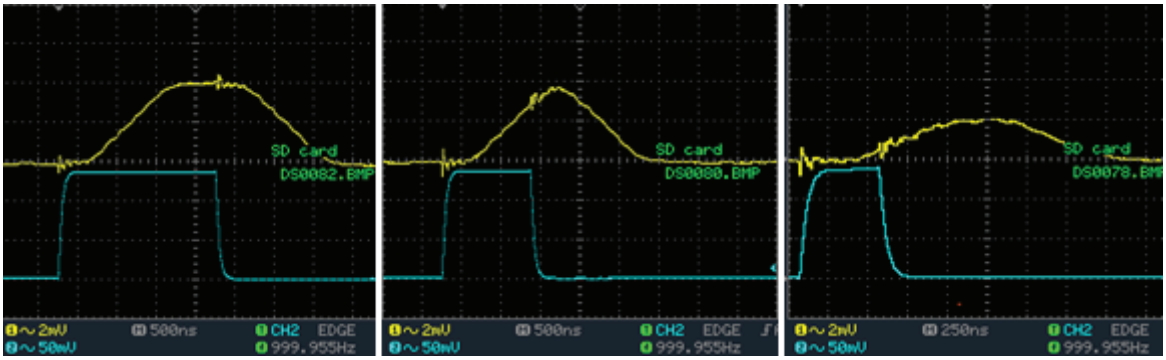

a b c

Figure 6. Current pulses (lower trace) and output signal of the sensor (upper trace) at T = (a) 2000, (b) 1120 and (c) 500 ns.

response (see Fig. 7b), which approaches the theoretical value $2\tau = 1120$ s at low values of T. The lag of the response behind the current (~400 ns) is due to both the above-mentioned instrumental factor and the light propagation time in the connecting line.

It follows from the above analysis that the shape of the response (the output signal of the FOCS) to a rectangular current pulse with $T < 2\tau$ allows one to correct the amplitude uncertainty in the measured pulse height, i.e. to convert $\Delta\varphi_h$ into $\Delta\varphi_H$ using time parameters of the response: $\Delta\varphi_H = \Delta\varphi_h(2\tau/T)$. It is worth noting that, according to Chen and Newson [8], at a known arbitrary current pulse shape one can obtain a relation for a decrease in uncertainty in pulse amplitude measurements using response shape parameters. In this study, this was confirmed experimentally for rectangular pulses.

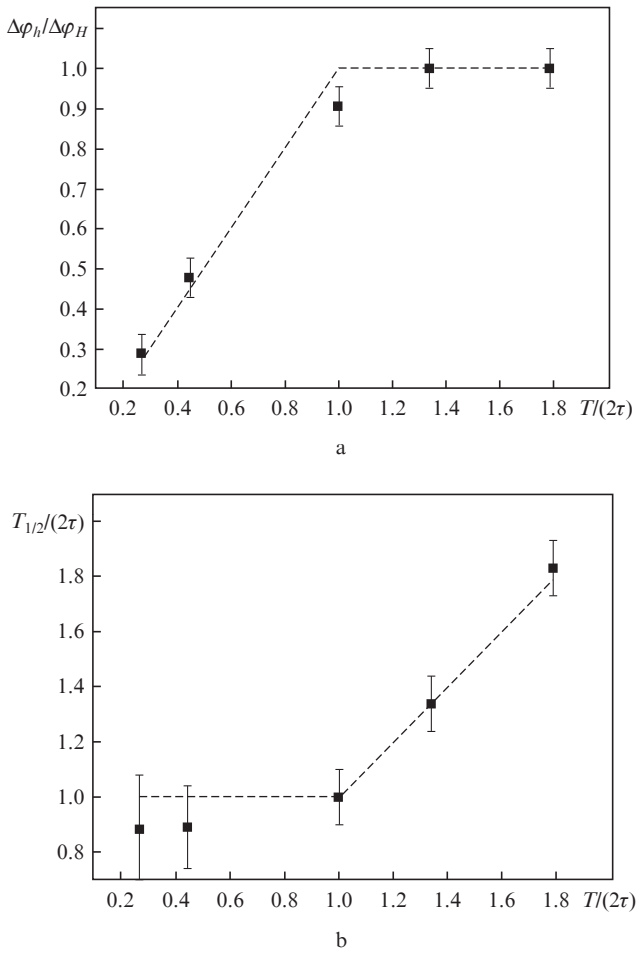

Figure 7. (a) Relative amplitude h/H and (b) relative full width at half maximum $T_{1/2}/(2\tau)$ of a detected current pulse as functions of the current pulse duration. The dashed lines represent calculation results.

The PMD in the connecting line has a relatively weak effect on the response shape at a line length corresponding to realistic experimental conditions. Below, we present our estimates for a 1-km-long connecting line:

1. Hi-bi line (L_b = 3 mm, λ = 1.55 μm). The delay between the slow and fast waves is $t_{sl} - t_f = l\lambda/(cL_b) = 1.72$ ns. Such a delay will distort the response at pulse durations $T < 10-20$ ns.

2. Spun line (L_b = 10 mm, L_s = 3 mm, λ = 1.55 μm). Calculation by formula (7) yields $t_{sl} - t_f = \Delta\varphi/\omega = 0.04$ ns, where $\Delta\varphi = \sigma\beta L/2$. In this case, the delay is even smaller.

6. Conclusions

Characteristics of the output signal of a Faraday effect fibre-optic current sensor in the detection of pulsed currents have been studied theoretically and experimentally. A distinctive feature of the described analysis is that spun fibre is considered as a sensing element of a sensor which is a part of a low-coherence reflective interferometer. We have investigated the influence of two physical mechanisms on the shape and magnitude of the pulsed response: transit mechanism, associated with the finite light propagation time in the sensing spun fibre, and polarisation mode dispersion in both the connecting line and spun fibre.

It has been shown that, in the case of a sharp change in current, the transit mechanism leads to a sensor response with linear edges and a duration determined by the relationship between the light propagation time in the spun fibre and the current pulse width and that the transition to a maximum response is not accompanied by any transient process. The experimentally observed additional transient process, of duration τ_{adj}, has an instrumental origin, and its influence causes no error in measurements of the maximum amplitude of a rectangular pulse of duration T provided that $T > \tau_{adj}$.

It has been shown theoretically that, in the case of a reflective interferometer, the PMD in the spun fibre of the sensing loop has to a first approximation no effect on response parameters, in contrast to the PMD in a connecting fibre (delay) line located before the sensing loop.

Appendix. Light propagation in a medium with a helical BR structure

An electromagnetic wave of optical light propagating in a weakly guiding circular dielectric fibre is known to have a predominantly transverse character. Because of this, in the vast majority of applied problems, one usually considers not the waveguiding fibre structure but an approximation in which plane waves propagate in a continuous medium. The refractive index of the medium is then taken to equal the effective refractive index of the fundamental mode of the fibre. Consider light propagation through spun fibre in this approximation.

In the case of a uniform helical structure of linear birefringence (for definiteness, a left-handed helical structure is considered) and a circular birefringence induced by an external magnetic field (Faraday effect), the transverse components of the dielectric permittivity tensor $\hat{\varepsilon}$, which appears in the material equations $\boldsymbol{D} = \hat{\varepsilon}\boldsymbol{E}$ and characterises the dielectric properties of the medium, have the form [17, 21, 22]

$$\hat{\varepsilon} = \bar{\varepsilon} + \mathrm{i}g\begin{pmatrix}0 & -1\\ 1 & 0\end{pmatrix} + \delta\begin{pmatrix}\cos 2\xi z & -\sin 2\xi z\\ -\sin 2\xi z & -\cos 2\xi z\end{pmatrix}, \tag{A1}$$

where $\bar{\varepsilon}$ is the average permittivity of the medium (with no allowance for its anisotropy), determined by the effective refractive index of the unperturbed fibre, $\bar{\varepsilon} = \bar{n}^2$, and $\xi = 2\pi/L_\mathrm{s}$ is the spatial angular rotation frequency of the linear birefringence axes with a pitch L_s. The constants δ and g, which determine the linear and circular birefringence, can be expressed through the corresponding differences between propagation constants, $\beta = k_y - k_x$ and $\gamma = k_r - k_l$, as $\{\delta, g\} = \{\beta, \gamma\}\,\bar{n}/k_0$.

In the general case, we consider a circular birefringence nonuniform in the light propagation direction and slowly varying with time, i.e. $g = g(t, z)$. If the variation in g is sufficiently slow, with $\Delta g/g \ll 1$, where Δg is the change during the oscillation period $T = 2\pi/\omega$, the time derivatives of $\hat{\varepsilon}$ can be neglected in deriving the wave equation. In view of this, the wave equation has the form

$$\frac{\partial^2 \boldsymbol{E}}{\partial z^2} = \frac{\hat{\varepsilon}\partial^2 \boldsymbol{E}}{c^2 \partial t}. \tag{A2}$$

A solution to this equation (in the case of plane waves propagating along the longitudinal axis z, $E_{x,y} = E_{x,y}(z)$ and $E_z = 0$) will be sought in the form of a combination of two circularly polarised waves [21]:

$$\boldsymbol{E} = A\boldsymbol{E}_0 \mathrm{e}^{\mathrm{i}(\omega t - kz)}, \quad \boldsymbol{E}_0 = \begin{pmatrix}E_\mathrm{l}\\ E_\mathrm{r}\end{pmatrix} = \begin{pmatrix}\mathrm{e}^{\mathrm{i}\xi z}\\ a\mathrm{e}^{-\mathrm{i}\xi z}\end{pmatrix}. \tag{A3}$$

Substituting the solution into (9), we obtain a system of equations for a and k:

$$\begin{aligned}(k-\xi)^2 &= k_0^2(\bar{n}^2 + g + a\delta),\\ (k+\xi)^2 &= k_0^2(\bar{n}^2 - g + a^{-1}\delta).\end{aligned} \tag{A4}$$

Note that Eqns (A4) are symmetric with respect to the transformation $k \to -k$ (propagation direction reversal), $g \to -g$ and $a \to 1/a$. Thus, knowing a general solution for a wave propagating in the forward direction, we can find the solution for a wave propagating in the backward direction by performing the above transformation.

Consider now an approximate solution at $\delta, g \ll \bar{\varepsilon}$ and at $\xi \ll k_0$ (i.e. in the case of a large spin pitch of the axes compared to the wavelength: $L_\mathrm{s} \gg \lambda$). A general solution to Eqn (A2) for waves propagating in the forward direction has the form of a linear combination of solutions of the form (A3) with the following coefficients:

$$\begin{aligned}a_{u,v} &= \frac{1}{\sigma}(-1 \pm \sqrt{\sigma^2+1}),\\ k_{u,v} &= k_0\bar{n}\left(1 \pm \frac{\delta}{2\bar{n}^2}\sqrt{\frac{1}{\sigma^2}+1}\right) = k_0\bar{n} \pm \frac{\Omega}{2},\end{aligned} \tag{A5}$$

where $\Omega = (2\xi+\gamma)\sqrt{1+\sigma^2} = \sqrt{(2\xi^2+\gamma)^2+\beta^2}$.

It follows from (A5) that, for $\sigma \leqslant 1$, we have $a_u \to 0$ (+ sign) and $a_v^{-1} \to 0$ (– sign). Thus, modes u and v are predominantly left and right circularly polarised, respectively. If these modes are considered, to a first approximation, as circularly polarised (quasi-circular), their refractive indices can be determined as

$$n_{u,v} \approx \frac{k_{u,v} \mp \xi}{k_0} = \bar{n} \pm \frac{\Omega - 2\xi}{2k_0} \approx \bar{n} \pm \frac{\beta\sigma}{4k_0} \pm \frac{\gamma}{2k_0}, \tag{A6}$$

where we use the expansion $\Omega \approx 2\xi + \beta\sigma/2 + \gamma$, valid at low values of σ. The corresponding wave equations in this approximation have the form

$$\frac{\partial^2 E_\mathrm{l,r}}{\partial z^2} = \frac{n_{u,v}^2}{c^2}\frac{\partial^2 E_\mathrm{l,r}}{\partial t^2}, \quad E_\mathrm{l,r} \approx 0. \tag{A7}$$

In conclusion, consider reflection of light waves from a mirror. Given the symmetry indicated above ($k \to -k$, $g \to -g$ and $a \to 1/a$), an incident predominantly left circularly polarised wave u with $k_u = \bar{n}k_0 + \Omega/2$ predominantly excites a right circularly polarised wave with $k_v' = \bar{n}k_0 - \Omega'/2$, and vice versa. Here, Ω' is equal to Ω with a change in the sign of γ. After reflection, the refractive indices of the waves transform as follows:

$$n_{u,v} \approx \bar{n} \pm \frac{\beta\sigma}{4k_0} \pm \frac{\gamma}{2k_0} \;\to\; n_{v,u}' \approx \bar{n} \mp \frac{\beta\sigma}{4k_0} \pm \frac{\gamma}{2k_0}. \tag{A8}$$

Therefore, when operating waves u and v are reflected from a mirror, the constant term in the refractive index due to the helical structure changes sign [the second terms in (A8)]. This means that, after wave propagation in the backward direction, the phase difference determined by the helical structure of the fibre is completely compensated. At the same time, the last term in (A8), determined by the circular birefringence induced in the medium, retains its sign upon reflection. As a result, light propagation in the backward direction doubles the Faraday phase shift between the waves.

References

1. Bohnert K., Gabus P., Kostovic J., et al. *Opt. Laser Eng.*, **43**, 511 (2005).
2. Starostin N.I., Ryabko M.V., Chamorovskii Y.K., et al. *Key Eng. Mater.*, **437**, 314 (2010).
3. Zhilin A.N., Lovchii I.L. *Trudy XII mezhdunarodnoi konf. "Prikladnaya optika-2016"* (Proc. XII Int. Conf. Applied Optics-2016) (St. Petersburg, 2016) Vol. 1, Section 3, p. 244.

4. Moreau Ph., Brichard B., Fil A., et al. *Fusion Eng. Des.*, **86**, 1222 (2011).
5. Pimenov A.V., Kazachkov Yu.P. RF Patent No. 2263709 (2005).
6. Kersey A.D., Bucholtz F., Dandridge A. *Int. J. Optoelectron.*, **3** (4), 323 (1988).
7. Gubin V.P., Morshnev S.K., Starostin N.I., et al. *Quantum Electron.*, **41** (9), 815 (2011) [*Kvantovaya Elektron.*, **41** (9), 815 (2011)].
8. Chen G.Y., Newson N.P. *Electron. Lett.*, **50** (8), 626 (2014).
9. Frosio G., Dändliker R. *Appl. Opt.*, **33** (25), 6111 (1994).
10. Blake J., Tantaswadi P., De Carvalho R.T. *IEEE Trans. Power Delivery*, **11** (1), 116 (1996).
11. Laming R.I., Payne D.N. *J. Lightwave Technol.*, **7** (12), 2084 (1989).
12. Gubin V.P., Isaev V.A., Morshnev S.K., et al. *Quantum Electron.*, **36** (3), 287 (2006) [*Kvantovaya Elektron.*, **36** (3), 287 (2006)].
13. Przhiyalkovsky Ya.V., Morshnev S.K., Starostin N.I., et al. *Quantum Electron.*, **43** (2), 167 (2013) [*Kvantovaya Elektron.*, **43** (2), 167 (2013)].
14. Przhiyalkovsky Ya.V., Morshnev S.K., Starostin N.I., et al. *Quantum Electron.*, **45** (11), 1075 (2015) [*Kvantovaya Elektron.*, **45** (11), 1075 (2015)].
15. Morshnev S.K., Gubin V.P., Vorob'ev I.L., et al. *Quantum Electron.*, **39** (3), 287 (2009) [*Kvantovaya Elektron.*, **39** (3), 287 (2009)].
16. Morshnev S.K., Gubin V.P., Przhiyalkovsky Ya.V., et al. *Quantum Electron.*, **43** (12), 971 (2013) [*Kvantovaya Elektron.*, **43** (12), 971 (2013)].
17. Zheleznyakov V.V., Kocharovskii V.V., Kocharovskii V.V. *Sov. Phys. Usp.*, **26**, 877 (1983) [*Usp. Fiz. Nauk*, **141** (10), 257 (1983)].
18. McIntyre P., Snyder A.W. *J. Opt. Soc. Am.*, **68** (2), 149 (1978).
19. Polynkin P., Blake J. *J. Lightwave Technol.*, **23** (11), 3815 (2005).
20. Kravtsov Yu.A., Orlov Yu.I. *Geometrical Optics of Inhomogeneous Media* (Berlin: Springer, 1990; Moscow: Nauka, 1973).
21. Belyakov V.A., Dmitrienko V.E., Orlov V.P. *Sov. Phys. Usp.*, **22**, 64 (1979) [*Usp. Fiz. Nauk*, **127** (2), 221 (1979)].
22. De Gennes P.G. *The Physics of Liquid Crystals* (Oxford: Clarendon, 1974; Moscow: Mir, 1977).